JOURNAL OF THE ROYAL SOCIETY Interface

J. R. Soc. Interface (2010) **7**, 1229–1241
doi:10.1098/rsif.2009.0534
Published online 11 February 2010

Characterization and analysis of carbon fibre-reinforced polymer composite laminates with embedded circular vasculature

C.-Y. Huang, R. S. Trask and I. P. Bond*

Advanced Composites Centre for Innovation and Science (ACCIS), Department of Aerospace Engineering, University of Bristol, Queen's Buildings, University Walk, Bristol BS8 1TR, UK

A study of the influence of embedded circular hollow vascules on structural performance of a fibre-reinforced polymer (FRP) composite laminate is presented. Incorporating such vascules will lead to multi-functional composites by bestowing functions such as self-healing and active thermal management. However, the presence of off-axis vascules leads to localized disruption to the fibre architecture, i.e. resin-rich pockets, which are regarded as internal defects and may cause stress concentrations within the structure. Engineering approaches for creating these simple vascule geometries in conventional FRP laminates are proposed and demonstrated. This study includes development of a manufacturing method for forming vascules, microscopic characterization of their effect on the laminate, finite element (FE) analysis of crack initiation and failure under load, and validation of the FE results via mechanical testing observed using high-speed photography. The failure behaviour predicted by FE modelling is in good agreement with experimental results. The reduction in compressive strength owing to the embedding of circular vascules ranges from 13 to 70 per cent, which correlates with vascule dimension.

Keywords: self-healing; biomimetic; vascular network; compression strength; high-speed photography

1. INTRODUCTION

Fibre-reinforced polymer (FRP) composites are gradually taking the place of metal alloys for significant parts of the primary structure in modern aircraft and their performance is key in determining reliability, performance, gross weight and cost-effectiveness of the vehicle (Ye *et al.* 2005). In such high-end applications, relatively minor damage within a composite material may result in a significant reduction in overall performance. Such damage may be difficult to detect visually and result in costly repair and maintenance work. The idea of self-healing may provide an alternative approach to addressing the damages caused by compression, modest impact, etc. The underlying concept of self-healing is analogous to the healing process in living organisms, i.e. to repair the internal damage by using the materials already contained within the structure (Trask *et al.* 2007*a*). Researchers in various fields (White *et al.* 2001; Kessler *et al.* 2003; Pang & Bond 2005; Toohey *et al.* 2007; Bond *et al.* 2008; Trask & Bond 2010) have successfully developed discrete bioinspired methods to provide autonomous repair functionality to targeted material systems, e.g. bulk polymers, FRP composites, etc. through liquid-encapsulated self-healing systems. However, such approaches are constrained by the limited supply of healing agent stored within the structure and hence failure to heal repeated or multiple damage events occurring at the same location. This is supported by Williams and co-workers (2009), in which the authors have demonstrated that, in a brittle thermoset matrix, crack propagation after healing occurs within the vicinity of the original damage site.

To address this problem, a concept for a next generation of self-healing composite materials is proposed which takes a biomimetic step forward and implements a pervasive vascular network system that has the potential to deliver healing agent from a central reservoir to all locations in the structure, as well as providing repeated healing for ongoing damage events (Trask *et al.* 2007*a*; Bond *et al.* 2008). Successful preliminary studies on such a biomimetic self-healing concept have been accomplished (Toohey *et al.* 2007, 2009; Williams *et al.* 2007) by embedding miniature interconnected vascular networks in either bulk polymeric materials or core materials of composite sandwich structures. The inclusion of the healing vascular networks has been shown not to disrupt the internal structure and performance of these materials as they can easily be made to conform and incorporate the embedded entities. However, this is not the case for advanced FRP composite laminates. The presence of such inclusions will disturb the composite laminate architecture, e.g. in-plane and out-of-plane fibre alignment, and can have a significant effect upon overall structural performance.

*Author for correspondence (i.p.bond@bristol.ac.uk).

Received 7 December 2009
Accepted 20 January 2010

An ongoing project at the University of Bristol aims to investigate the conceptual form of vascular network designs which bestow a self-healing capability on a FRP composite laminate, as well as evaluating the implications on composite mechanical performance of including such networks. In order for a self-healing composite laminate to be considered for application in aerospace and other high-performance fields, it must be shown that such inclusions do not result in significant degradation in mechanical performance of the host material (i.e. strength, modulus, etc.). Behaviour under compressive loading is studied as this reflects a critical load regime for self-healing of the polymer matrix.

The conceptual design of engineered vascular networks can be divided into two length scales: the vascule cross-sectional shape (micro-scale) and the planform vascular pattern (meso-scale), respectively. The former refers to the individual vascule cross-sectional geometry, while the latter refers to the whole vascular morphology, ranging from two-dimensional planar networks, as presented in the studies of Bejan and co-workers (2006), Emerson *et al.* (2006), Janakiraman *et al.* (2007), Trask *et al.* (2007*b*) and Williams *et al.* (2007), to three-dimensional interconnected configurations, as reported in Toohey and co-workers (2007), Williams *et al.* (2008), Kim *et al.* (2009) and Toohey *et al.* (2009). This paper considers only the former. The reader is referred to Bejan & Lorente (2008) for more detailed reviews of vascular morphological design.

It is difficult to envisage forming an interconnected vascular network within a FRP laminate without having certain sections of the network being oriented off-axis to the local fibre direction(s) of adjacent plies. Thus, when a vascule with a dimension much greater than a typical reinforcing fibre is embedded off-axis to the local fibre orientation, the result is a geometric distortion of the surrounding fibres and creation of *resin-rich pockets*, as shown in figure 1. Such resin pockets are regarded as potential defects within the structural laminate (Silva *et al.* 2005). This study focuses on the case where the vascule is oriented *orthogonal* to the local fibre direction as this is regarded as having the most detrimental consequences for the structural integrity of the host laminate.

The fundamental form of a vascule cross-section is a simple circle (figure 1). Advancing from the circular form, several different vasculature patterns can be considered for their feasibility as part of a self-healing system, including single and multiple vascule forms, respectively. Novel multiple vascular forms include adjacent circular vascules and bioinspired 'ray cell' features. The purpose of designing multiple vascule forms is to host multi-component healing agents currently under consideration for self-healing composite materials (Williams *et al.* 2009). As a first step in this research direction, this paper considers only an investigation of unidirectional (UD) *single circular* vascules. Studies on multiple vascular forms will be presented in a subsequent paper.

In this study, both the size and shape of a single vascule (diameter range 150–400 μm) can be compared with a typical fibre-optic sensor (FOS; typical diameter 100–300 μm). Therefore, previous studies on the consequences of embedding FOS into FRP composite laminates (e.g. Case & Carman 1994; Friebele *et al.* 1999; Zhou *et al.* 2004; Silva *et al.* 2005; Shivakumar & Bhargava 2005; Fernando & Degamber 2006; Kousourakis *et al.* 2008) are regarded as good comparators. Jensen and colleagues (1992*a*,*b*) are among the pioneers to study the influence upon host composite performance following embedment of FOS with regard to orientation and numbers of FOS. Subsequent researchers concluded that the degradation of material strength and modulus is significantly affected by the optical fibre diameter, the FOS orientation relative to nearest plies and the FOS materials (Friebele *et al.* 1999; Zhou *et al.* 2004; Fernando & Degamber 2006). Apart from modifying the diameter and constituent materials of FOS in order to reduce their influence on resulting performance, it is the resin-rich pocket caused by off-axis FOS embedment that draws the attention of most researchers. The presence of resin pockets results in a high internal stress concentration that is detrimental to the overall structure. Their geometry is mainly determined by FOS diameter, orientation, laminate stacking sequence, laminate stiffness and lamination pressure (Case & Carman 1994). Experimental and analytical studies have reported that the presence of resin pockets has a significant effect on the host material's performance under static, fatigue and impact loading. The scale of reduction under compressive loading ranges from 15 to 60 per cent of original strength, while for bending and tension the influence is negligible (Shivakumar & Emmanwori 2004; Silva *et al.* 2005). The reduction under fatigue loading is between 20 and 35 per cent (Benchekchou & Ferguson 1998; Silva *et al.* 2005). Such findings are further supported by research on inclusion of other features (e.g. hollow galleries; Kousourakis *et al.* 2008). In all these studies, whether the inclusions are FOS or hollow galleries, a circular cross-section is assumed.

One of the major differences between a hollow vascule and an FOS is that the former has no load-carrying capability. A hollow vascule may thus act as a significant defect within the structure. Very little literature is available which reports the studies of such hollow inclusions.

This paper presents a study of the influence of circular hollow vascules upon the mechanical performance of the host material. Manufacturing methods for the creation of one-dimensional circular hollow vascules within a conventional carbon fibre-reinforced polymer (CFRP) composite laminate system (Hexcel IM7/8552) are proposed. Optical microscopy was used to precisely characterize the laminate cross-sectional geometries, especially within the lenticular resin pocket region. Such detailed quantification tasks are an essential preliminary activity. These quantification results are used for subsequent construction of finite element (FE) models (using ABAQUS 6.7-1). The FE modelling results of stress–strain analysis in this region while the laminate is under static compressive load are presented, and likely failure mechanisms are proposed based on the FE results. Finally, in-plane compressive tests were conducted to validate the failure mechanisms deduced

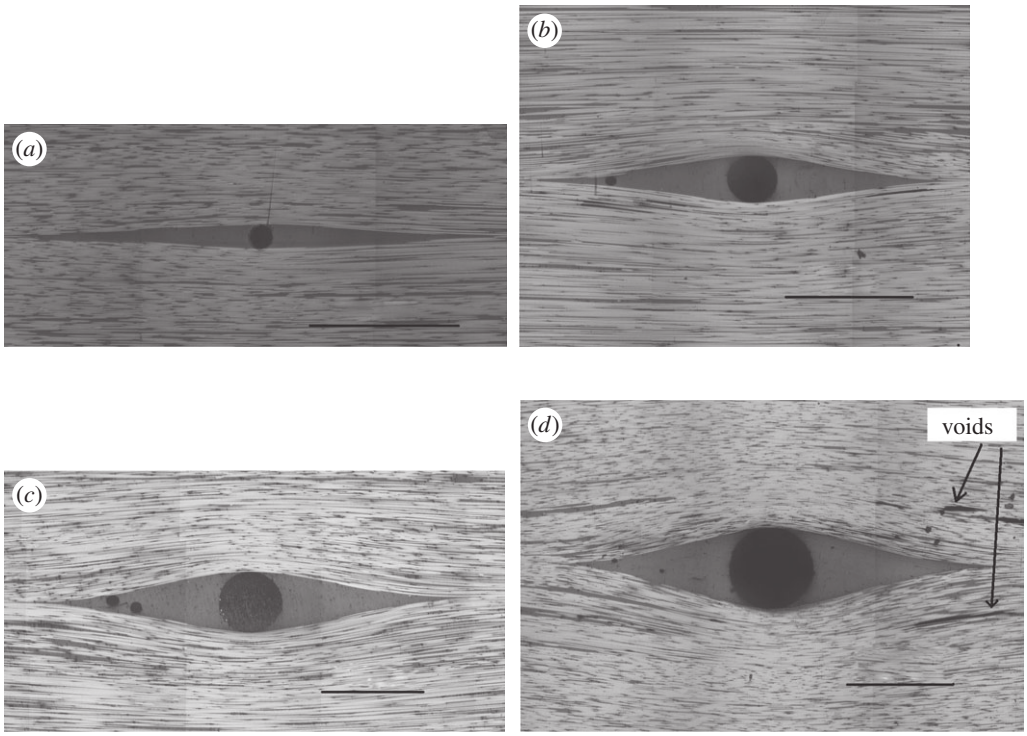

Figure 1. Cross-sectional optical micrographs of circular vascules (diameters of (*a*) 80 μm, (*b*) 200 μm, (*c*) 310 μm and (*d*) 400 μm) forming a resin-rich pocket in a CFRP laminate. Scale bars, 500 μm.

from finite element analysis (FEA). In particular, an understanding of the role played by the resin pockets in crack initiation at or near the vascule was required. The compressive testing was recorded by high-speed photography (HSP) in order to precisely capture the failure mechanism. A comprehensive comparison between FEA prediction and experimental results is provided.

2. MATERIAL AND METHODS

2.1. Specimen manufacture

Specimens of UD carbon fibre/epoxy composite laminates were prepared containing vascules of various dimensions along the laminate mid-plane, oriented perpendicular to the fibre direction. The laminates were made using 24 plies (3 mm thickness) or 32 plies (4 mm thickness) of UD IM7/8552 prepreg tape (HexPly 8552, Hexcel Ltd, UK) with dimensions of 600 × 150 mm. The vascule-forming precursors used in this study were stainless steel wires that are commercially available in various diameters. The stainless steel wires have high rigidity and high melting temperature. This is in direct contrast to Trask & Bond (2010), in which low melting temperature channel-forming materials (i.e. solder wires) were used, resulting in a slightly elliptical channel cross-section (see Trask & Bond 2010). The stainless steel wires maintain reasonably identical cross-sectional shape after the autoclave cycle. Dimensional details of all specimens studied are given in table 1. A 32-ply stack was chosen to host the largest circular vascules in order to ensure that the laminate surface remained flat after curing, i.e. ply disturbance in through-thickness direction caused by the presence of large inclusions is mitigated by a greater ply stack.

Table 1. Detailed dimensions of vascular specimens.

vascule diameter (μm)	laminate ply (thickness)
80, 150, 200, 310, 400 and 560	24 plies (3 mm)
710	32 plies (4 mm)

In order to assist their later removal from cured laminates, a thin polytetrafluoroethylene (PTFE) film was manually coated onto the surface of the stainless steel wires. This was undertaken by mounting the wires horizontally in air, rotating at a constant rate, and manually applying a PTFE spray (ROCOL PTFE spray, part no. 72021) from a distance of approximately 20–30 cm (recommended by the manufacturer) for two complete revolutions. After the coating, the wires were introduced at the mid-layer of the prepreg stack, along the centreline of the specimen. The wires were aligned perpendicular to the fibre orientation and extended over the entire width of the specimen. A small amount of tension was applied to the wires by adhering both ends to the tool plate surface to ensure their straightness. The prepreg stack was then covered in non-porous peel-ply, and a steel caul plate overlaid to ensure surface flatness and smoothness before being sealed in a vacuum bag and cured in an autoclave following the manufacturer's (Hexcel Ltd, UK) specified cycle (6 h at 180°C at 700 kPa). After the laminates were cured, the steel wires were removed manually, leaving hollow-channel

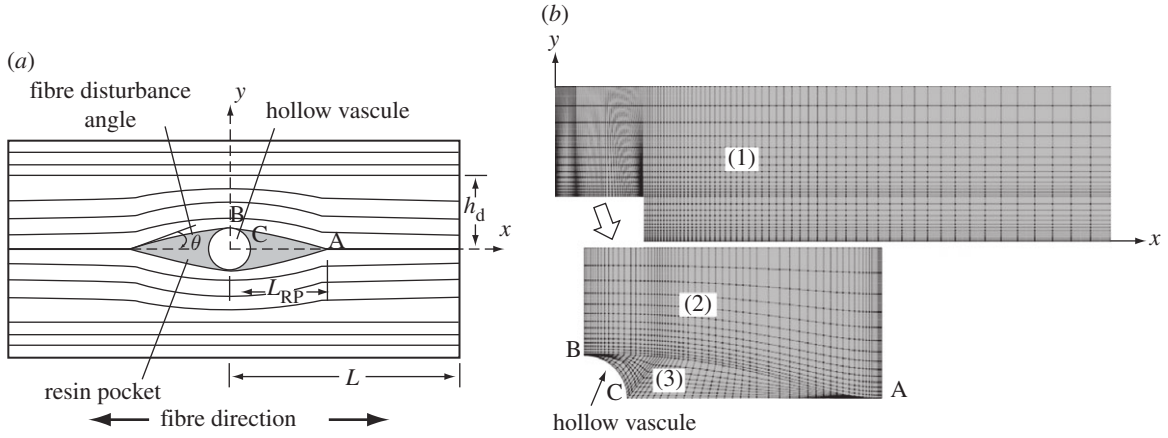

Figure 2. (*a*) Conceptual model of laminate with embedded circular vascule surrounded by a resin pocket; (*b*) quarter section of an idealized FE model which is divided into three distinct regions.

vascules. Unwanted laminate edges were trimmed, and test specimens were cut to two different sizes: 30 × 30 mm, and 90 mm (fibre direction) × 10 mm (width). The former were mounted in Prime 20LV epoxy resin (Gurit (UK) Ltd), polished and optically examined to characterize laminate microstructures. The latter were stored for subsequent mechanical testing in compression.

2.2. Microscopic characterization of resin pocket geometrical parameters

Mounted composite specimens were examined using optical microscopy (Olympus GX41 microscope with Pixera Pro 150ES camera and Olympus SZX16 microscope with ColorView camera). For each vascular dimension, four to five specimens were prepared and micrographed and average measurements of these specimens were obtained.

The two-dimensional conceptual models of a single circular vascule are illustrated in figure 2, which are idealized from real micrographs (e.g. figure 1). As indicated in figure 2*a*, the following five parameters for the resin pocket region of each vascule type were quantified from the cross-sectional micrographs using image analysis software (ImageJ v. 1.41).

— *Resin pocket length* (L_{RP}). Defined as the planar distance from the vascule centre to the end of the resin-rich pocket. Two values of L_{RP} were obtained from each micrograph and averaged.
— *Fibre disturbance angle* (θ_d). Defined as the angle subtended by the resin pocket with the plane of the local fibre ply.
— *Fibre disturbance height* (h_d). Defined as the separation distance from the axis of the resin pocket (and also the vascule) to the first layer of reinforcing fibres that are observed to be undisturbed by the presence of the inclusion. Note that these are visual observations and the results are approximate measures.
— *Resin pocket area* (A). The cross-sectional area of the resin pocket, including the vascule(s). An average value was obtained for each vascule.

2.3. Finite element modelling methodology

Since model geometry and applied in-plane load are symmetric, only one-quarter of the conceptual model (figure 2*a*) is considered, with the centre point of the central vascule being taken as the origin, as shown in figure 2*b*. The length (or UD fibre direction), the thickness and the width of laminate are taken as x-, y- and z-axes of the model in figure 2*b*, respectively. The idealized model is divided into three zones and the material properties in different zones are varied. The area of interest, i.e. zones (2) and (3), is enlarged. Since the laminate length of manufactured specimens (90 mm) is much larger than the vascule diameter, the default length of all models has been set as $50r$, which is long enough to avoid any unnecessary boundary effects. To simulate the worst scenario vascule orientation, i.e. vascules aligned at 90° to local fibre direction, vascule orientation of all models is parallel to the z-axis, or out of the paper direction. The curved lines in zone (2) represent the profile of disturbed reinforcing fibres because of embedded vascules, which are geometrically distributed as per the micrographs. The fibre orientations in zone (2) are varied to follow the shape of the resin pocket before reverting to being parallel with the x-axis. Zone (1) is undisturbed composite laminate and zone (3) is the resin-rich pocket. The material properties (including elastic, thermal and failure properties) of IM7/8552 composite laminate and Hexcel 8552 neat epoxy resin system applied to different zones in the FE modelling tasks are detailed in appendix A.

The specimen width is very large when compared with its thickness, hence the model is assumed to be in a plain strain state. The FE models are mapped with 8-node plain strain quadrilateral elements (CPE8) by applying an isoparametric mapping concept using a commercial FE code ABAQUS 6.7-1. Extra care was taken when meshing the regions of interest such as vascule boundaries and resin pocket run-outs. Linear elastic analysis is performed and symmetric boundary conditions are applied to both x- and y-axes. Default loading of 1.650 GPa (σ_0) is applied to the model edge ($x = 50r$) equal to a 1 per cent strain for a UD IM7/8552 composite laminate. For each principal

Table 2. Geometric parameters of circular vascules, with the coefficient of variation in parentheses.

vascule diameter, $2r$ (μm)	resin pocket length, L_{RP}	fibre disturbance height, h_d	fibre disturbance angle, θ_d (°)	resin pocket area, A (μm^2)	lay-up system
80	$18.01r$ (6.3%)	$4.0r$ (6.3%)	3.09 (6.6%)	5.7×10^4	24 plies
150	$13.77r$ (8.9%)	$3.89r$ (4.4%)	4.26 (3.7%)	1.48×10^5	24 plies
200	$6.84r$ (7.1%)	$3.49r$ (3.8%)	7.86 (4.3%)	1.63×10^5	24 plies
310	$5.45r$ (5.9%)	$3.79r$ (2.4%)	9.56 (7.2%)	3.03×10^5	24 plies
400	$5.08r$ (3.7%)	$3.71r$ (5.7%)	9.85 (5%)	3.96×10^5	24 plies
560	$3.99r$ (4.1%)	$3.19r$ (3.9%)	13.31 (1.4%)	7.57×10^5	24 plies
710	$3.78r$ (4.5%)	$3.06r$ (4.8%)	16.58 (4.4%)	9.74×10^5	32 plies

direction (longitudinal and through-thickness), complete stress and strain contours are obtained.

According to the standard curing cycle suggested by the manufacturer, the laminates are cured at 180°C and then cooled down to ambient temperature (20°C). The first 30°C of cooling has little influence on the curing stresses since the material's viscoelastic relaxation is still at a high level (Garstka *et al.* 2007). Therefore, the temperature decrease from 150°C to ambient is taken into account as a thermal effect when obtaining the curing stresses in the FEA. The modelling thus contains two consecutive steps. The curing stresses because of temperature decrease are obtained in the first step. Mechanical loading is then applied to the model in step 2 to calculate the mechanical response. Currently, the self-healing functionality proposed to exploit these vascular inclusions is targeted at recovery of compressive strength following impact damage. Therefore, a compressive loading, which results mainly in matrix-dominated failure, has been chosen as the primary mechanical loading applied in the FE models.

In order to ensure the convergence of the modelling results, three different meshing densities were generated and their results evaluated. The numbers of elements/nodes of each mesh are: (A) 1277/7548; (B) 3975/12 240; and (C) 4796/18 510, respectively. It was found that the best convergence was obtained with mesh density (B), while mesh density (C) provided similar results but with unnecessary excess computation. Mesh density (B), therefore, is used for all FE modelling tasks in this study.

2.4. Mechanical testing with high-speed photography

The compression testing was conducted in a 100 kN Instron mechanical test machine under displacement control at 1 mm min^{-1}, following the test method developed by Haberle & Matthews (1994). The test arrangement and the compression rig design are illustrated in detail in Haberle & Matthews (1994). The specimen planar dimension is 90 mm (length, UD fibre direction) by 10 mm (width). Laminates of 24 plies (nominal thickness 3 mm) were used to host hollow vascules with size 80–560 μm; while 32-ply laminates (nominal thickness, 4 mm) were used for the 710 μm vascules. In order to fully appreciate the failure mechanisms, only one vascule is embedded within each test specimen. In addition, plain 24-ply composite laminates (i.e. no embedded vascule) were tested to serve as a baseline for compression strength. All laminate samples were cut from large composite panels that were manufactured following standard processes suggested by the material manufacturer. The laminates were cut to desired size using a water-cooled diamond saw and roughened at both ends by using a sand blaster. Glass fibre-reinforced epoxy end tabs (Heathcote Industrial Plastics) were attached to the laminates with Araldite 2015 epoxy resin adhesive, in accordance with the test method (Haberle & Matthews 1994). For each vascule type, 5–12 replicates were tested and the load–displacement results were recorded by the test machine control software and averaged afterwards.

In order to capture the instant of crack initiation, a Photron Fastcam SA1 high-speed digital video camera (8 Gb memory) was employed to monitor the complete testing cycle. The recording frame rate was 150 000 frames per second (fps), which provides a maximum record time of 2.24 s. Under normal conditions such elapse time and frame rate are enough to capture the whole process from crack initiation to final failure. Manual triggering was used for the test because of the absence of automatic triggering between the high-speed camera and test machine.

3. RESULTS AND DISCUSSIONS

3.1. Microscopic characterization of resin pocket geometrical parameters

Micrographs of different diameter circular vascules, enclosed by lenticular resin-rich pockets, are presented in figure 1. In some micrographs, voids can be found either within the resin pocket or between adjacent plies of reinforcing fibres. It can be easily observed from the micrographs that both the fibre disturbance angle and resin pocket area are proportional to vascule diameter, in accordance with Dasgupta *et al.* (1992).

The measured geometric parameters for all circular vascules are listed in table 2. Note that for ease of subsequent FE modelling tasks, two major parameters, resin pocket length (L_{RP}) and fibre disturbance height (h_d), are specifically normalized by the radius of the vascule, r. Most of the vascules (more than 95%) measured from the micrographs have the same cross-sectional dimensions as the original vascule-forming steel wires, eliminating concerns about mismatch between coefficients of thermal expansion during cure. A positive correlation between vascule diameter and each geometric parameter can be observed in table 2.

These trend lines suggest that embedding larger vascules results in larger resin-rich pockets as well as more disturbed/curved reinforcing fibres. This is likely to have a greater implication for structural integrity. These observations show good agreement with the reported results for FOS (Shivakumar & Emmanwori 2004) and hollow vascules formed by solder wires (Trask & Bond 2010). Such agreement suggests that the observations presented in this paper are generally applicable to other CFRP laminate systems.

Of all the parameters listed in table 2, the resin pocket length (L_{RP}) is predicted to have the most direct influence on structural integrity of the laminate. There is a dichotomy in which larger vascules will carry a greater volume of healing agent thus offering a potentially greater self-healing capability, whereas larger L_{RP} arising from larger vascules would require greater crack propagation through a resin pocket to interact with a vascule and trigger the healing process. It can be observed from table 2 that when embedded vascules are larger than 200 μm, the resin pocket lengths (L_{RP}) remain in the range of four to six times the vascule radius. Such a consistent trend may provide a useful guideline for material engineers to deduce an optimized point between self-healing capacity and self-healing efficiency.

The fibre disturbance angle has little direct influence upon any healing capacity utilizing embedded vascules; however, it will greatly affect the overall mechanical performance of the material as it may increase the structure's vulnerability towards micro-buckling while under compressive loading. Since both the default loading directions in the corresponding analytical and mechanical studies are parallel to the fibre direction (or x-axis), the fibre disturbance angle in this case can be regarded as fibre misalignment angle with respect to loading. In the past decade, numerous studies (Wisnom & Atkinson 2000; Yokozeki *et al.* 2005; Vinet & Gamby 2008) have been undertaken to analyse the effects of fibre waviness, fibre misalignment and fibre micro-buckling on the mechanical performance of either UD or woven composite materials, especially under compressive loading. Various analytical and empirical models have been proposed, and the agreed consensus is that fibre misalignment angle has a dramatic effect on material performance. The influence of misalignment angle can be nonlinear, with even a small misalignment angle leading to a significant reduction in compressive strength of the material (Wisnom & Atkinson 2000). The distribution and randomness of such wavy fibres also have obvious influence.

The pressure applied during autoclave cure generally removes any perturbations in the ply stacks, resulting in smooth and flat composite panels. The fact that no thickness changes are visible indicates that embedding such big inclusions into composite laminates results in not only disturbance of local fibre orientation, but local increases in fibre volume fraction in the through-thickness direction (Trask & Bond 2010). This inevitably affects the local stress–strain distributions and the overall structural performance (Pilkey 2008). To this end, the 'fibre disturbance height' (h_d) is a good indication of the local fibre volume fraction changes and is regarded as one of the essential parameters for analysing structural performance. Positive correlation between h_d and vascular dimension in table 2 suggests that larger vascules may result in greater regions of increased fibre volume fraction above and below the vascule. This can also be regarded as a disadvantage of embedding larger vascules into FRP laminates.

The resin pocket area is directly related to the dimensions of the embedded vascule. During cure, the resin is transferred from the laminate prepreg stack into the space created by an embedded vascule to form the resin pocket. Therefore, according to the principle of mass conservation, the presence of a resin pocket means that some other regions of the composite laminate must contain a lower volume of matrix material than the initial value. However, the presence of the steel wire vascule preforms causes an uneven local pressure distribution during consolidation resulting in small voids in the host laminate adjacent to the resin-rich pockets. A larger vascule gives rise to larger voids within the adjacent composite laminate, effectively becoming significant structural defects (figure 1). This observation corresponds with the findings of Trask & Bond (2010). Under loading, such voids are likely to initiate crack formation or attract a nearby propagating crack away from interacting with a vascule, a key requirement if used for a self-healing function.

3.2. Finite element analysis

To match the compression testing results presented in later sections, the FEA results of laminates with a 400 μm circular vascule are presented here as the representative of all configurations studied. The resin pocket length $L_{RP} = 5.08r$, and the fibre disturbance height $h_d = 3.71r$. Since the FE models are predefined as in plain strain, only two principal strains (ε_1 and ε_2) are generated, as no out-of-plane strain occurs. The stress contours in the longitudinal (i.e. fibre direction, σ_1) and transverse (i.e. through the thickness, σ_2) directions are shown in figure 3*a*,*b*, respectively. The longitudinal (ε_1) and transverse (ε_2) strain contours are shown in figure 3*c*,*d*, respectively. Here only the regions of interest, i.e. resin pocket and curved laminates (zones (2) and (3) in figure 2), of each stress–strain contour are presented in order to provide a more illustrative comparison. The stress concentration factors (SCFs) for various locations of all vascular sizes are listed in table 3.

It can be observed in figure 3 that under axial compressive load, the longitudinal stress concentration occurs at the boundary of the resin pocket (point D), near the top end of circular vascule (point B). The average applied axial compressive load at the model edge is 1.65 GPa, which is denoted as σ_0. The longitudinal SCF at point D, or $K_{1(D)}$, is calculated as $\sigma_1/\sigma_0 = 2.79$ (figure 3*a*). Note that, here the notations 1 and 2 refer to longitudinal and through-thickness directions, respectively; while the notations A, B, C and D refer to specific points as denoted in figure 3. In the through-thickness direction, it can be seen that the highest *tensile* stress in the transverse direction occurs at the vascular boundary, point C (or position at

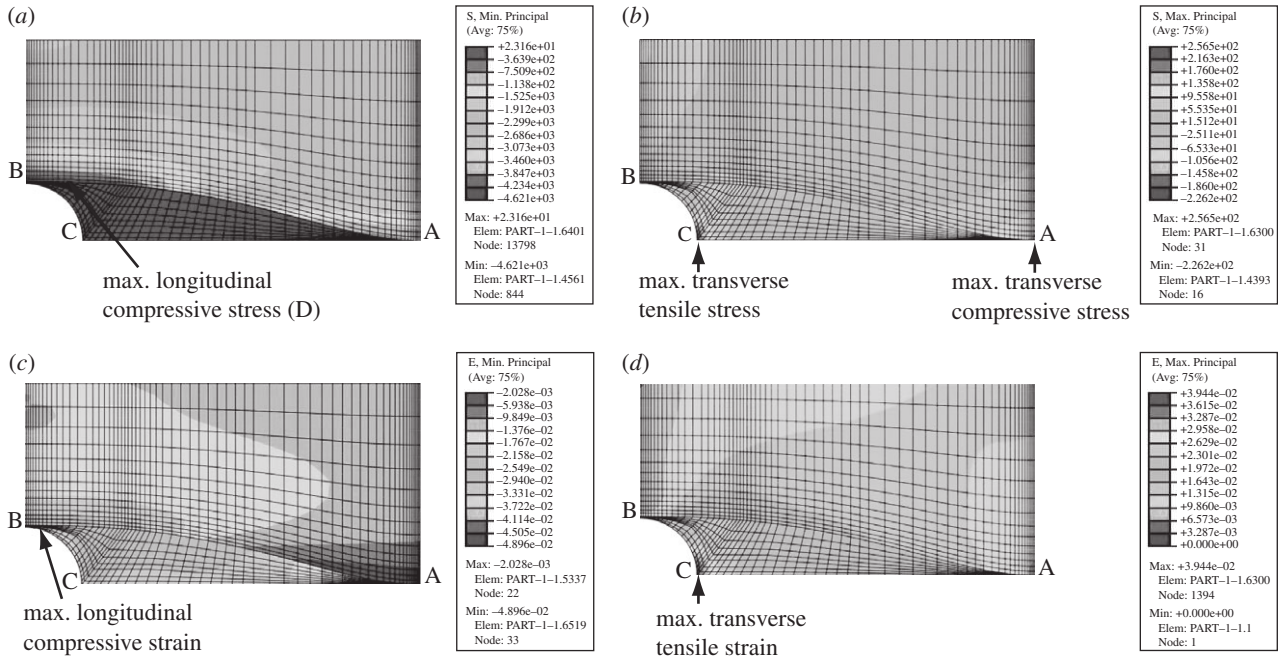

Figure 3. (*a*) Longitudinal stress contour; (*b*) transverse stress contour; (*c*) longitudinal strain contour; and (*d*) transverse strain contour, around a 400 μm vascule.

Table 3. Stress concentration factors at various locations for all vascule diameters studied (where K means stress concentration factor; notations 1, 2 refer to longitudinal and through-thickness direction, respectively; notations A, B, C and D refer to specific locations in figure 3).

	through-thickness SCF		longitudinal SCF	
vascule size (μm)	$K_{2(A)}$	$K_{2(C)}$	$K_{1(B)}$	$K_{1(D)}$
80	0.117	−0.084	1.18	1.28
150	0.122	−0.099	1.28	1.44
200	0.128	−0.133	1.91	2.01
310	0.133	−0.145	2.30	2.43
400	0.137	−0.155	2.55	2.79
560	0.144	−0.177	3.30	3.39
710	0.156	−0.190	3.79	3.91

3 o'clock) with an SCF (σ_2/σ_0) of −0.155, or $K_{2(C)}$. The highest *compressive* stress occurs at the resin pocket run-out region, i.e. point A with an SCF of 0.137, or $K_{2(A)}$. Note that the minus sign for SCF indicates that the resulting stress is in the opposite direction to applied stress. The through-thickness tensile stresses are regarded as the main cause of crack initiation within conventional FRP laminates because of relatively low strength in this matrix-dominated direction compared with the fibre direction (Shivakumar & Bhargava 2005; Silva *et al.* 2005). It can, therefore, be deduced that internal cracks may be initiated at the vascule boundary (position at 3 o'clock) when the structure is under axial compression. Proposed material compressive failure mechanism from these FEA results is presented in later sections.

In the fibre direction (figure 3*c*), the average strain in the laminate region, i.e. zone (1), is about 1 per cent. The location of maximum strain concentration is very close to point B, which is at the boundary of the resin pocket and normal laminate ply. This is not far from the location of maximum stress concentration. In the transverse direction (figure 3*d*), the maximum tensile strain occurs again at point C, which corresponds well with the stress contours.

Note that with regard to stress–strain contours, all vascules have shown similar trends regardless of vascule dimensions. Hence, only the contours of 400 μm are presented.

Since the stress distributions are of primary interest in the current study, only the stress results will be presented in the following sections. It can be concluded from the stress–strain contours that critical stresses (maximum or minimum) occur at the x-axis or at the resin pocket boundary (the curved line 'BDA' as shown in figure 3*a*). As a result, stress variations along these paths are further examined for detailed understanding. The plots in figure 4 are re-plotted data exported from ABAQUS and post-processed in MS Office Excel 2007. To simplify the variation, the x-axes in all plots are shown as normalized distance from either the centre of the hollow vascule (figure 4*b*,*c*) or point B (figure 4*d*); while the y-axes refer to stress components divided by σ_0 to become SCFs.

Figure 4*b* shows the variation of normalized σ_x along the model x-axis. There is very low longitudinal stress (σ_x) in the resin pocket region, which increases significantly moving into the composite region, because of the substantial change in material stiffness. Similar trends were also found by Shivakumar & Bhargava (2005). Moving towards the end of model ($x = L$), σ_x converges to σ_0 and finally the SCF reaches unity.

The variation of σ_y along the model x-axis is shown in figure 4*c*. The stress within the vascule region remains zero because of the absence of any load-bearing

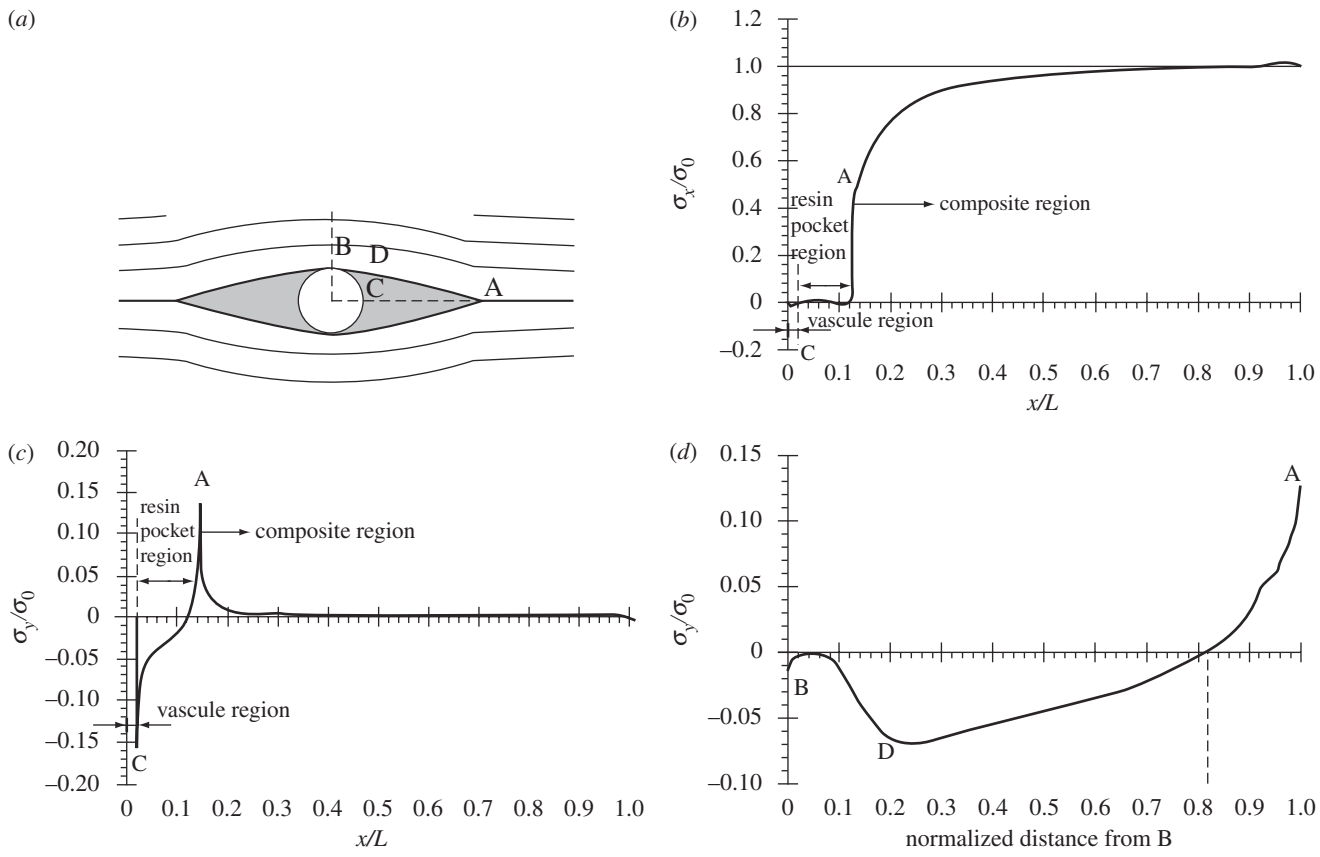

Figure 4. (*a*) Notation of points A–D of FE models; (*b*) $\boldsymbol{\sigma}_x$ along *x*-axis; (*c*) $\boldsymbol{\sigma}_y$ along *x*-axis; and (*d*) $\boldsymbol{\sigma}_y$ along path BDA, for a 400 μm vascule.

material. Two obvious peaks are observed at points C and A, respectively. These two peaks denote maximum stress concentrations in opposing directions. Under compressive load, a maximum negative peak of reactive stress at point C refers to the highest transverse tensile stress. The distinct stress variation also indicates that the section close to point A experiences compressive stress, while the section close to point C is under tensile loading. These results contrast with the findings of Shivakumar & Bhargava (2005) because of the different embedded material properties.

The variation of $\boldsymbol{\sigma}_y$ along the path 'BDA' is presented in figure 4*d*. The negative maximum point located close to point D is the maximum stress concentration in the longitudinal direction; while the positive maximum occurs at point A. Similar to figure 4*c*, distinct positive/negative regions can be observed from the plot, with a transition point at about 80 per cent of the distance from point B. Such a transition point varies from 65 to 85 per cent according to vascule size, but plots show a similar trend. A similar deduction can be made from this plot in that under compressive load the area nearest the resin pocket run-out will experience compressive stress, while the area near the vascule will experience tensile stress.

3.3. Deduced failure mechanisms based on FEA results

From the FEA results, failure mechanisms of laminates with embedded hollow vascules under compressive loads can be deduced. Specific failure mechanisms, as shown in figure 5, are as follows.

Under axial compressive loading, a transverse tensile stress is concentrated at point C, while compressive stress peaks at point A (figure 5*b*). The transverse tensile stresses around the hollow vascule (points B and C) may result in two failure modes. When the laminate mode I fracture toughness (G_{Ic}) is greater than the fracture toughness of the resin pocket or neat resin ($G_{\mathrm{c(resin)}}$), the failure will be initiated at point C in the form of cracking, leading to steps (c) and (d). Otherwise, if $G_{\mathrm{c(resin)}} > G_{\mathrm{Ic}}$, delamination occurs at the resin pocket boundaries, leading to steps (e) and (f). It is dependent on the specific composite system under investigation as to which failure mode is more likely to happen.

In the first case (figure 5*c*,*d*), the high transverse tensile stress at C may initiate cracking at the vascule boundary when (Shivakumar & Bhargava 2005)

$$\boldsymbol{\sigma}_0 \geq \frac{S_{22\mathrm{T}}}{K_{2(\mathrm{C})}}, \tag{3.1}$$

where $S_{22\mathrm{T}}$ is transverse tensile strength and $K_{2(\mathrm{C})}$ is transverse SCF at point C.

The concentrated tensile stress at C is released when the vascule is ruptured. Once the cracks are formed, they propagate toward the ends of the resin pocket owing to the transverse tensile stress at the new crack front, C′. This is potentially beneficial for a self-healing delivery system based on vascular networks since the healing agents stored within a vascule have the

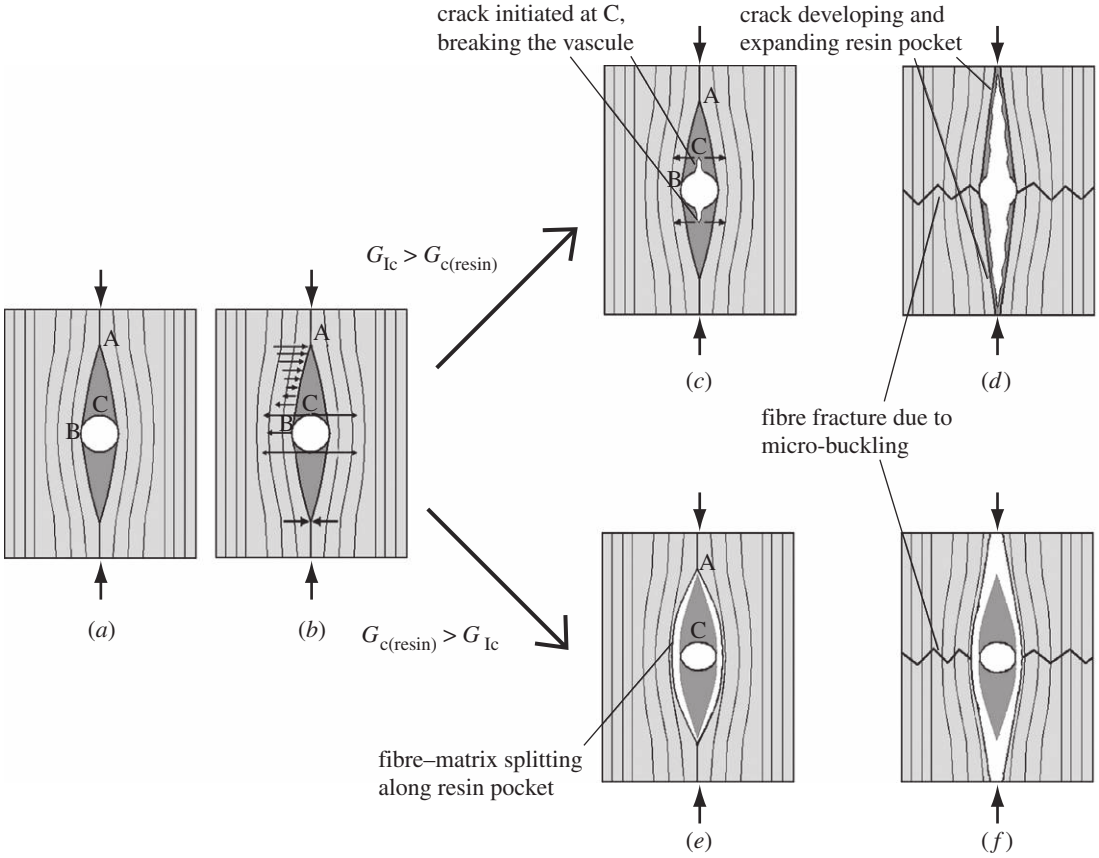

Figure 5. Deduced failure mechanism under compressive load.

potential to heal the crack and terminate/delay the structural failure process. Upon continued compression, the propagation of the crack opens the resin pocket and further increases the fibre misalignment of the surrounding laminate plies. The local compression strength is thus reduced since it is a function of the fibre misalignment angle (Budiansky & Fleck 1993). Finally, the composite fails because of fibre micro-buckling around the vascule region (point B), as shown in figure 5*d*. This happens when the longitudinal compressive strength of the material is reached (Shivakumar & Bhargava 2005), or

$$\sigma_0 \geq \frac{S_{11C}}{K_{1(B)}}, \tag{3.2}$$

where S_{11C} is transverse tensile strength and $K_{1(B)}$ is the longitudinal SCF at point B.

According to these criteria and the SCF results obtained from FEA, the predicted stress at crack initiation and final failure for each vascular dimension are calculated and will be compared with the experimental results in a later section.

When $G_{Ic} > G_{c(resin)}$ (figure 5*e*,*f*), splitting between resin pocket and surrounding laminates occurs. This is likely to initiate at point B and then propagate towards the resin pocket run-out, as shown in Shivakumar & Bhargava (2005). The fibre misalignment is thus enlarged, resulting in a reduction in the material's compressive strength. Again, upon continued loading, the crack propagates along the edge of the resin pocket and into the adjacent ply interface. Finally, the structure fails because of micro-buckling of fibres around the vascules.

Such failure mechanisms differ from that observed in FOS laminates as, in that case, the resin pocket surrounds a solid fibre instead of a hollow vascule. As a result, the transverse tensile stress is concentrated at point B, instead of point C, and will initiate the interfacial failure around point B (Shivakumar & Emmanwori 2004). Eventually, the material fails because of fibre buckling; this result concurs with the prediction in this study.

3.4. Compression test results

The aim of the mechanical testing is to validate the fidelity of the FEA results and consequent failure mechanisms. For the compression testing, vascules of 80, 150, 200, 310, 400 and 560 μm, respectively, were tested. In addition, five baseline specimens (i.e. no embedded vascule) were also tested to measure the compressive strength of the baseline laminate. Limited by optical resolution, the HSP was unable to catch detailed crack propagation for smaller vascules, including 80 and 150 μm, respectively. For each vascule size tested, 5–12 specimens were tested while being recorded by HSP. The HSP recording time varies from 1.8 to 2.24 s with maximum frame rate of 150 000 fps. Because of a complicated and delicate manufacturing technique, it was found much more difficult to produce specimens with 80 μm vascules compared with the larger diameters. During the mechanical removal process from cured laminates, some 80 μm stainless steel wires were

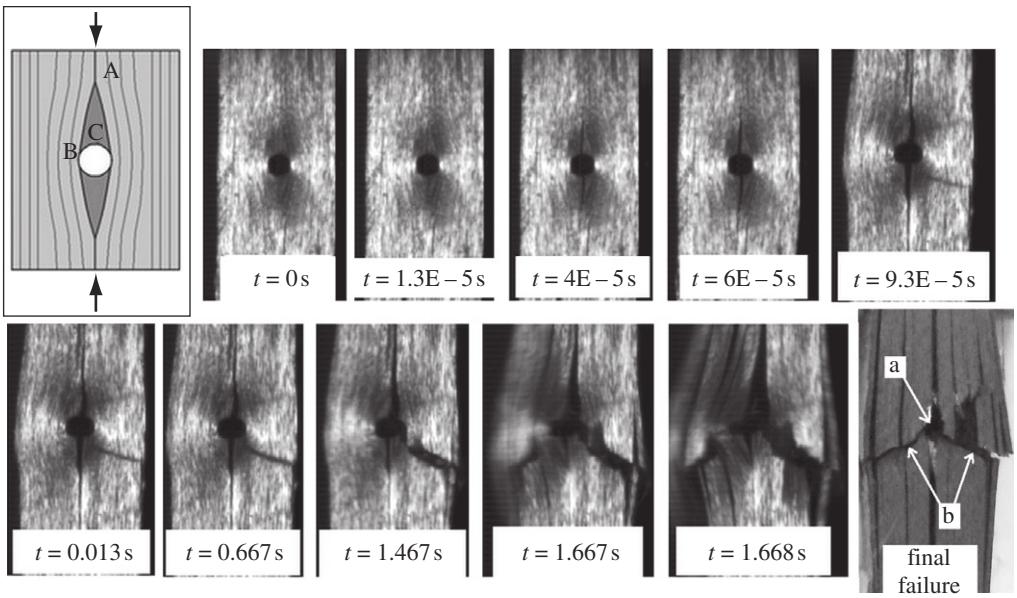

Figure 6. Pictures taken by HSP during axial compression testing of CFRP with a 400 μm embedded vascule. The first image (top left) denotes the specimens' orientation and the resin pocket location. The last image (bottom right) shows final failure with 'a' denoting location of circular vascule and 'b' denoting through-thickness V-shaped fracture.

Table 4. Comparison of FEA predictions and experimental results (with coefficient of variation in parentheses), including the relative compressive strengths of each vascule size.

	crack initiation (GPa)		final failure (GPa)			
vascule diameter (μm)	prediction	experiment	prediction	experiment	relative strength	sample
baselines	—	—	—	1.298 (2.1%)	100%	5/5
80	0.714	n.a.	1.270	1.120 (7.5%)	87%	4/5
150	0.603	n.a.	1.171	0.807 (4.2%)	62%	6/8
200	0.451	0.492 (7.1%)	0.789	0.733 (1.4%)	56%	8/10
310	0.414	0.431 (9.2%)	0.651	0.610 (1.9%)	47%	10/12
400	0.387	0.419 (10.2%)	0.536	0.503 (3.2%)	39%	9/12
560	0.339	0.321 (6.5%)	0.441	0.393 (3.8%)	30%	9/11

fractured. This left part of the wire preform within the laminate panel, and thus blocked the vascule. Following specimen preparation, the specimens containing blocked (or partially blocked) vascules were excluded from the subsequent test programme.

Figure 6 shows the photos taken by HSP during the compression test of a 400 μm vascule specimen. Several pictures are combined to present a continuous progression from $t = 0$ (frame no. 1) to $t = 1.668$ s (frame no. 250020), along with the final failure scene (taken by conventional digital camera). Limited by the optical capability, the image resolution is less than perfect but good enough for distinguishing the appearance of cracks. The fibre orientation is in the vertical direction in all images. The black circular hole in the centre is the hollow vascule with the two resin pocket regions above and below the vascule. It can be clearly affirmed from the frame of '$t = 4\text{E}-5$ s' that the cracks initiate at the vascule boundary (position at 3 o'clock in the FE model). Upon continued loading, the cracks propagate towards both ends of the resin pocket ('$t = 6\text{E}-5$ s'). The first through-thickness crack appears at '$t = 9.3\text{E}-5$ s' and the cracks continue to grow with further loading. Eventually the composite laminate fails by buckling, having V-shaped or oblique fracture surfaces, as shown by the last image in figure 6.

Such a compression failure mechanism corresponds with the progress of crack initiation, crack propagation and final failure illustrated previously and as predicted by FEA findings. The majority of the specimens (over 80%) tested have shown similar failure behaviour (table 4) regardless of vascule size. Other failure phenomena include cracking within the end tab regions and failure far away from the resin pocket region, etc. Overall, the fidelity of the FE models has been verified.

In addition, it can also be confirmed that with the IM7/8552 composite laminate, the compression failure mechanism (a)–(b)–(c)–(d) shown in figure 5 is more representative than (a)–(b)–(e)–(f). That is, $G_{c(\text{resin})} > G_{Ic}$ for the IM7/8552 material.

The point of crack initiation is difficult to precisely determine, as has been reported by other researchers (Ye *et al.* 2005; Kousourakis *et al.* 2008). Hence, the coefficient of variation of crack initiation stress is

generally larger than final failure stress. The experimental results for each vascule dimension are compared with predictions based on FEA in table 4.

3.5. Comparison of FEA predictions and experimental results

Table 4 lists the full comparison of FEA predictions and mechanical test results for stress at crack initiation and final failure, respectively. The FEA predictions are obtained from equations (3.1) and (3.2) for crack initiation stress and final failure stress, respectively. The measured compressive strength of baseline laminates (i.e. no vascule) is 1.298 GPa, which is lower than that reported in the literature (Jumbo *et al.* 2007), 1.5 GPa (S_{11C} in appendix A). Different testing and manufacturing methods may account for the apparent difference in strength. In addition, the relative compressive strengths of each vascule diameter from the baseline value, i.e. 1.298 GPa, are included.

For both the FEA and experimental data in table 4, an apparent decrease can be observed in both crack initiation and failure stress with increased vascule size. In the FEA predicted results, crack initiation stress is between 60 and 75 per cent of final failure; while experimental crack initiation stress ranges from 70 to 80 per cent of failure strength. Generally, the FEA crack initiation stress is closer to the experimental data than the predicted final strength. Such a difference is understandable since the FEA is based on a continuous model under application of load, whereas in the experimental testing the structural micromechanics undergo significant change as the damage propagates. Thus, more sophisticated FEA models will be required to obtain more accurate predictions. Notwithstanding the shortcomings of the FEA undertaken to date, the models are able to provide a composite engineer with a basic tool for gauging the likely influence of hollow vascules within CFRP composite laminates.

It is also worth noting the reduction in compressive strength with the inclusion of hollow vascules within a laminate. Reductions in compressive strength ranging from 13 per cent (80 μm) to 70 per cent (560 μm) have been observed. The testing of the 710 μm vascules is omitted since the trend is observable from the results for 80–560 μm vascules. The huge strength reduction on samples containing large vascules is unsurprising as these inclusions possess nominal dimensions up to four times an individual ply thickness (i.e. 125 μm) within a laminate, which is highly sensitive to any disturbance of its well-organized fibre architecture. Even with the smallest inclusion, i.e. 80 μm vascule which has nominal dimension only two-thirds of individual ply thickness, a strength reduction of 13 per cent can be seen. Such findings agree with the compressive strength reductions reported in the FOS studies, which found a range of values from 30 to 70 per cent, depending on FOS orientation, laminate thickness, host composite, etc. (Jensen *et al.* 1992*b*; Friebele *et al.* 1999; Shivakumar & Emmanwori 2004; Kousourakis *et al.* 2008). Note that the last column in table 4 indicates the proportion of laminate specimens failed in 'predicted failure mode' (i.e. specimens failed in the resin pocket regions) out of total specimens tested. In general, over 75 per cent of tested specimens have shown failure within the resin pocket regions.

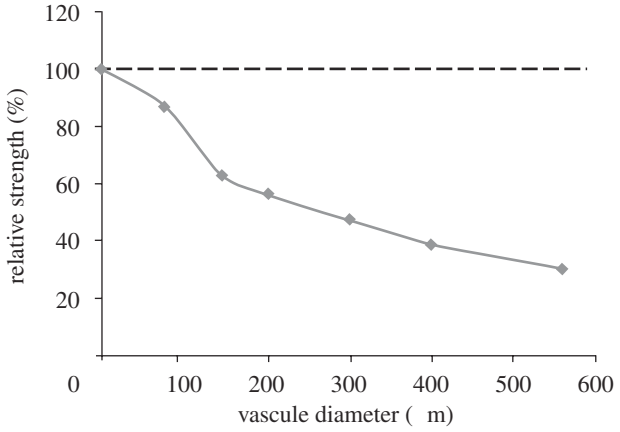

Figure 7. Relative compressive strengths versus vascule diameter.

The decreasing trend of the relative compressive strengths in table 4 is further plotted in figure 7. An interesting trend can be observed in figure 7 that the compressive strength reduction is modest for smaller vascule diameters (i.e. 80 μm) but is significant for the vascule dimensions greater than 150 μm. i.e. 13 versus greater than 35 per cent. These results suggest that a threshold value could exist below 80 μm that has negligible detrimental effect. Conversely, as the vascule diameter becomes large (greater than 400 μm) the negative effect is severe but tends towards being asymptotic. Such maximum and minimum threshold values may differ in different material systems. A similar finding has been reported by Kousourakis and co-workers (2008).

4. CONCLUDING REMARKS

A preliminary study of a next generation of bioinspired self-healing composite materials with embedded vasculatures is presented. Manufacturing methods to create hollow vascules within CFRP composite laminates have been proposed. Embedding these vascules in FRP composite laminates, off-axis with respect to the local fibre orientations, results in the creation of lenticular resin-rich pockets and local geometric disturbance of the fibre reinforcement. A series of cross-sectional micrographs of these lenticular resin pockets have been produced. Based on the micrographs, empirical relationships between the vascular diameter and resin pocket geometry have been established. These relationships are based on observations of vascular features within an IM7/8552 carbon/epoxy composite laminate system; such trends may be applicable to other similar composite systems. Two-dimensional FE models were generated according to these microscopic observations. The FEA has shown that under axial compression, cracks will be initiated at the vascule boundary at a 3 o'clock position owing to through-thickness tensile stress concentration. The cracks propagate towards the apex of the resin pocket and then into the laminate while further loading is applied. Final failure occurs

owing to fibre micro-buckling. Such failure mechanisms are beneficial with regard to the proposed self-healing function since the healing process can be triggered by the crack propagating through the vascule before structural failure. Compression testing results that are recorded using HSP have validated the FEA models proposed. The FEA results are in good agreement with the experimental data regarding crack initiation stress but overestimate failure strength. The reduction in experimentally determined compression strength because of the presence of circular vascules ranges from 13 to 70 per cent, depending on vascule diameter. These results provide a basic 'toolbox' for designing an advanced functional FRP composite laminate, e.g. for the purposes of self-healing, thermal management, etc., whereby the vascular dimensions can be tuned/tailored to rupture at desired loads.

APPENDIX A. MATERIAL PROPERTIES OF IM7/8552 COMPOSITE LAMINATES

IM7/8552 elastic properties (Jumbo *et al.* 2007)	
E_{11T}	165 GPa
E_{11C}	145 GPa
E_{22T}	11.38 GPa
E_{22C}	10.20 GPa
E_{33T}	11.38 GPa
E_{33C}	10.20 GPa
G_{12}	5.12 GPa
G_{23}	5.12 GPa
G_{13}	3.92 GPa
υ_{12}	0.3
υ_{23}	0.487
υ_{13}	0.3
Hexcel 8552 neat epoxy elastic properties	
E	4.67 GPa
υ_{12}	0.35
IM7/8552 thermal properties (Krueger *et al.* 2001)	
α_{11}	$6 \times 10^{-7}\,\mathrm{K}^{-1}$
α_{22}	$2.86 \times 10^{-5}\,\mathrm{K}^{-1}$
α_{33}	$2.86 \times 10^{-5}\,\mathrm{K}^{-1}$
α (neat resin)	$5.0 \times 10^{-5}\,\mathrm{K}^{-1}$
IM7/8552 failure properties (Jumbo *et al.* 2007)	
longitudinal tensile strength (S_{11T})	2.6 GPa
longitudinal compressive strength (S_{11C})	1.5 GPa
transverse tensile strength (S_{22T})	60 MPa
transverse compressive strength (S_{22C})	290 MPa
shear strength (S_S)	90 MPa

REFERENCES

Bejan, A. & Lorente, S. 2008 *Design with constructal theory*. Hoboken, NJ: Wiley.

Bejan, A., Lorente, S. & Wang, K.-M. 2006 Networks of channels for self-healing composite materials. *J. Appl. Phys.* **100**, 033 528. (doi:10.1063/1.2218768)

Benchekchou, B. & Ferguson, N. S. 1998 The effect of embedded optical fibers on the fatigue behaviours of composite plates. *Comp. Struct.* **41**, 113–120. (doi:10.1016/S0263-8223(98)00034-8)

Bond, I. P., Trask, R. S. & Williams, R. 2008 Self-healing fiber-reinforced polymer composites. *MRS Bull.* **33**, 770–774.

Budiansky, B. & Fleck, N. A. 1993 Compressive failure of fibre composites. *J. Mech. Phys. Solids* **41**, 183–211. (doi:10.1016/0022-5096(93)90068-Q)

Case, S. W. & Carman, G. P. 1994 Compression strength of composites containing embedded sensors or actuators. *J. Intell. Mater. Syst. Struct.* **5**, 4–11. (doi:10.1177/1045389X9400500101)

Dasgupta, A., Wan, Y. & Sirkis, J. S. 1992 Prediction of resin pocket geometry for stress analysis of optic fibers embedded in laminated composites. *Smart Mater. Struct.* **1**, 101–107. (doi:10.1088/0964-1726/1/2/001)

Emerson, D. R., Cieślicki, K., Gu, X. & Barber, R. W. 2006 Biomimetic design of microfluidic manifolds based on generalized Murray's law. *Lab Chip* **6**, 447–454. (doi:10.1039/b516975e)

Fernando, G. F. & Degamber, B. 2006 Process monitoring of fibre reinforced composites using optical fibre sensors. *Int. Mater. Rev.* **51**, 65–106. (doi:10.1179/174328006X79481)

Friebele, E. J. *et al.* 1999 Optical fiber sensors for spacecraft applications. *Smart Mater. Struct.* **8**, 813–838. (doi:10.1088/0964-1726/8/6/310)

Garstka, T., Ersoy, N., Potter, K. D. & Wisnom, M. 2007 In situ measurements of through-the-thickness strains during processing of AS4/8552 composite. *Composites A* **38**, 2517–2526. (doi:10.1016/j.compositesa.2007.07.018)

Haberle, J. G. & Matthews, F. L. 1994 An improved technique for compression testing of unidirectional fibre-reinforced plastics; development and results. *Composites* **25**, 358–371. (doi:10.1016/S0010-4361(94)80006-5)

Janakiraman, V., Mathur, K. & Baskaran, H. 2007 Optimal planar flow network designs for tissue engineered constructs with built-in vasculature. *Ann. Biomed. Eng.* **35**, 337–347. (doi:10.1007/S10439-006-9235-0)

Jensen, D. W., Pascual, J. & August, J. A. 1992*a* Performance of graphite/bismaleimide laminates with embedded optical fibers. Part I: uniaxial tension. *Smart Mater. Struct.* **1**, 24–30. (doi:10.1088/0964-1726/1/1/004)

Jensen, D. W., Pasaual, J. & August, J. A. 1992*b* Performance of graphite/bismaleimide laminates with embedded optical fibers. Part II: uniaxial compression. *Smart Mater. Struct.* **1**, 31–35. (doi:10.1088/0964-1726/1/1/005)

Jumbo, F., Ruiz, P. D., Yu, Y., Swallowe, G. M., Ashcroft, I. A. & Huntley, J. M. 2007 Experimental and numerical investigation of mechanical and thermal residual strains in adhesively bonded joints. *Strain* **43**, 319–331.

Kessler, M. R., Sottos, N. R. & White, S. R. 2003 Self-healing structural composite materials. *Composites A* **34**, 743–753. (doi:10.1016/S1359-835X(03)00138-6)

Kim, S., Lorente, S., Bejan, A., Miller, W. & Morse, J. 2009 The emergence of vascular design in three dimensions. *J. Appl. Phys.* **103**, 123 511. (doi:10.1063/1.2936919)

Kousourakis, A., Bannister, M. K. & Mouritz, A. P. 2008 Tensile and compressive properties of polymer laminates containing internal sensor cavities. *Composites A* **39**, 1394–1403. (doi:10.1016/j.compositesa.2008.05.003)

Krueger, R., Paris, I. L., O'Brien, T. K. & Minguet, P. J. 2001 Fatigue life methodology for bonded composite skin/stringer configurations. NASA technical report NASA/TM-2001-210842, ARL-TR-2432.

Pang, J. W. C. & Bond, I. P. 2005 A hollow fibre reinforced polymer composite encompassing self-healing and enhanced damage visibility. *Composites Sci. Technol.* **65**, 1791–1799. (doi:10.1016/j.compscitech.2005.03.008)

Pilkey, W. D. 2008 *Peterson's stress concentration factors*, 3rd edn. Hoboken, NJ: Wiley.

Shivakumar, K. & Emmanwori, L. 2004 Mechanics of failure of composite laminates with an embedded fiber optic sensor. *J. Comp. Mater.* **38**, 669–680. (doi:10.1177/0021998304042393)

Shivakumar, K. & Bhargava, A. 2005 Failure mechanics of a composite laminate embedded with a fibre optic sensor. *J. Comp. Mater.* **39**, 777–798. (doi:10.1177/0021998305048156)

Silva, J. M. A., Devezas, T. C., Silva, A. P. & Ferreira, J. A. M. 2005 Mechanical characterization of composites with embedded optical fibers. *J. Comp. Mater.* **39**, 1261–1281. (doi:10.1177/0021998305050423)

Toohey, K. S., Sottos, N. R., Lewis, J. A., Moore, J. S. & White, S. R. 2007 Self-healing materials with microvascular networks. *Nat. Mater.* **6**, 581–585. (doi:10.1038/nmat1934)

Toohey, K. S., Hansen, C. J., Lewis, J. A., White, S. R. & Sottos, N. R. 2009 Delivery of two-part self-healing chemistry via microvascular network. *Adv. Funct. Mater.* **19**, 1399–1405. (doi:10.1002/adfm.200801824)

Trask, R. S. & Bond, I. P. 2010 Bioinspired engineering study of plantae vascules for self-healing composite structures. *J. R. Soc. Interface* **7**, 921–931. (doi:10.1098/rsif.2009.0420)

Trask, R. S., Williams, H. R. & Bond, I. P. 2007*a* Self-healing polymer composites: mimicking nature to enhance performance. *Bioinspir. Biomim.* **2**, 1–9. (doi:10.1088/1748-3182/2/1/p01)

Trask, R. S., Williams, G. J. & Bond, I. P. 2007*b* Bioinspired self-healing of advanced composite structures using hollow glass fibres. *J. R. Soc. Interface* **4**, 363–371. (doi:10.1098/rsif.2006.0194)

Vinet, A. & Gamby, D. 2008 Prediction of long-term mechanical behaviour of fibre composites from the observation of micro-buckling appearing during creep compression tests. *Comp. Sci. Technol.* **68**, 526–536. (doi:10.1016/j.compscitech.2007.06.032)

White, S. R., Sottos, N. R., Geubelle, P. H., Moore, J. S., Kessler, M. R., Sriram, S. R., Brown, E. N. & Viswanathan, S. 2001 Autonomic healing of polymer composites. *Nature* **409**, 794–797. (doi:10.1038/35057232)

Williams, H. R., Trask, R. S. & Bond, I. P. 2007 Self-healing composite sandwich structures. *Smart Mater. Struct.* **16**, 1198–1207. (doi:10.1088/0964-1726/16/4/031)

Williams, H. R., Trask, R. S., Knights, A. C., Williams, E. R. & Bond, I. P. 2008 Biomimetic reliability strategies for self-healing vascular networks in engineering materials. *J. R. Soc. Interface* **5**, 745–747. (doi:10.1098/rsif.2007.1251)

Williams, G. J., Bond, I. P. & Trask, R. S. 2009 Compression after impact assessment of self-healing CFRP. *Composites A* **40**, 1399–1406. (doi:10.1016/j.compositesa.2008.05.021)

Wisnom, M. R. & Atkinson, J. W. 2000 Fibre waviness generation and measurement and its effect on compressive strength. *J. Reinf. Plastics Comp.* **19**, 96–110. (doi:10.1106/MYQG-T534-UPA5-RPFK)

Ye, L., Ye, L., Su, Z. & Meng, G. 2005 Functionalized composite structures for new generation airframes: a review. *Comp. Sci. Technol.* **65**, 1436–1446. (doi:10.1016/j.compscitech.2004.12.015)

Yokozeki, T., Ogasawara, T. & Ishikawa, T. 2005 Effects of fibre nonlinear properties on the compressive strength prediction of unidirectional carbon-fibre composites. *Comp. Sci. Technol.* **65**, 2140–2147. (doi:10.1016/j.compscitech.2005.05.005)

Zhou, G., Sim, L. M., Brewster, P. A. & Giles, A. R. 2004 Through-the-thickness mechanical properties of smart quasi-isotropic carbon/epoxy laminates. *Composites A* **35**, 797–815. (doi:10.1016/j.compositesa.2004.01.018)